Nonlinear theory of pattern formation in ferrofluid films at high field strengths

J. Richardi* and M. P. Pileni†

Laboratoire des Matériaux Mésoscopiques et Nanométriques, UMR CNRS 7070, Université Pierre et Marie Curie (Paris VI), Boîte Postal 52, 4, place Jussieu, 75230 Paris Cedex 05, France

(Received 10 April 2003; published 26 January 2004)

When a magnetic field is applied to a thin layer of a suspension of magnetic nanoparticles (ferrofluid), the formation of labyrinthine and hexagonal patterns is observed. We introduce a theory to describe ferrofluid patterns at high field, where a nonlinear relationship between field and magnetization is expected. The computational difficulties due to the use of a nonlinear magnetization curve are solved by a reformulation of the magnetic energy equation. The evolution of the pattern size at intermediate and very high fields can be understood by an analysis of limiting cases of the magnetization curve. In particular, at a very high field the pattern size reaches a constant saturation value which has been recently confirmed by experiments. The field for the onset of a nonlinear behavior is shifted to higher field strength due to a demagnetization effect. This can partially explain the ability of linear approaches to reproduce experimental data even at a high field. Finally, the impact of the nonlinearity of the magnetization curve on the transition between hexagonal and labyrinthine patterns is discussed.

DOI: 10.1103/PhysRevE.69.016304 PACS number(s): 47.54.+r, 47.65.+a, 77.84.Nh

I. INTRODUCTION

Ferrofluids are colloidal suspensions of magnetic nanoparticles in a liquid solvent [1]. These magnetic liquids exhibit a large number of extraordinary properties. A phenomenon which has received considerable attention, both experimentally and theoretically, is the so-called labyrinthine instability [2,3]. A ferrofluid is confined with an immiscible nonmagnetic liquid between two closely spaced glass plates (Hele-Shaw cell). The application of a uniform magnetic field at right angles to the glass plates induces a labyrinthine pattern of several millimeters: the convoluted black walls made of the ferrofluid are separated by paths of the transparent nonmagnetic liquid. This magnificent instability was observed for the first time in the late 1970s [2]. The initial theoretical studies focused on the conditions necessary to establish the labyrinthine patterns [2]. In 1983, Rosensweig *et al.* [3] proposed a theory to calculate the labyrinthine stripe width as a function of the cell height and the field strength. Their theoretical results were apparently in good agreement with the experimental data [3,4]. In the following years, experimental studies showed that, under certain conditions, hexagonal arrays of ferrofluid columns appear instead of labyrinthine patterns [5,6]. Due to the use of demixed ferrofluids, the size of the patterns were markedly reduced to several micrometers [5,7]. Structures similar to those in ferrofluids were also observed in magnetorheological suspensions [8,9]. The dynamics of the pattern formation and the transition between hexagonal and labyrinthine structures were studied, both theoretically and experimentally [6,7,10–16]. The occurrence of similar patterns in other systems, such as Langmuir monolayers and type I superconductors, has been the subject of several theoretical investigations [17].

The theoretical approaches are usually based upon the formulation of the free energy as a sum of magnetostatic and interfacial parts [1–3]. Recent theoretical studies also include an entropy term, which might prove important in determining the size of patterns for micron-sized cell heights [10,11]. Approximations [2,3] were proposed to simplify the computation of the magnetic energy. Although these methods are widely used nowadays [6,10,12–16] the effects of the approximations upon the calculated results were only recently studied [18,19]. We have shown that, in particular, the approximation introduced by Rosensweig *et al.* [3] leads to markedly overestimated stripe widths at high field strengths [4]. The good agreement with experimental data observed before was due only to errors in the computation of the theoretical values which were corrected in Ref. [4]. Moreover, the method proposed by Rosensweig *et al.* [3] predicts field-induced transitions between hexagonal and labyrinthine patterns which are not confirmed using more accurate theories [18]. Therefore, we have recently developed an alternative approximate scheme that is very efficient and gives values in good agreement with the accurate results [19].

Our interest in these kinds of theories was motivated by the discovery of labyrinthine and hexagonal mesostructures of magnetic cobalt nanocrystals in our laboratory [20,21]. They have been obtained by the evaporation of solutions of cobalt nanocrystals while applying a magnetic field perpendicular to the substrate. These artificial structures of several hundreds of nanometers can be manipulated to achieve tailored materials for applications and for exploration of physical phenomena. Our aim is to develop a theory, which explains the formation of these mesostructures. Moreover, we want to find the parameters which control their size and their morphology. One major obstacle to this theory is the linear relationship between the magnetization and the magnetic field usually assumed in published approaches. Figure 1 shows the magnetization curve $M(H)$ of a deposition of co-

*Electronic address: richardi@sri.jussieu.fr

†Electronic address: pileni@sri.jussieu.fr; URL: http://www.sri.jussieu.fr; to whom all correspondence should be sent.

 ©2004 The American Physical Society

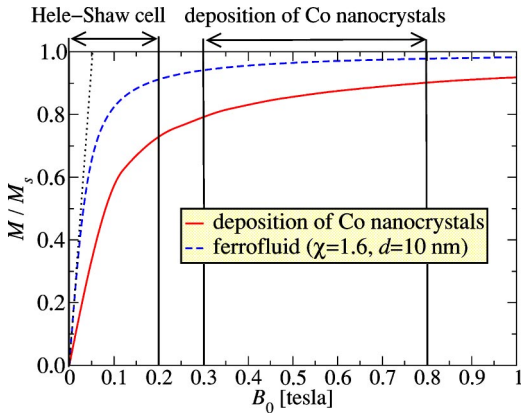

FIG. 1. Magnetization curves. Solid line: experimental curve of a deposition of cobalt nanoparticles [21]; dashed line: Langevin function of a ferrofluid (magnetite particles with a diameter of 10 nm, initial magnetic susceptibility of 1.6); dotted line: linear approximation of this Langevin function. The arrows indicate the range of fields used for the experiments by Rosensweig *et al.* [3] (Hele-Shaw cell) and by Germain *et al.* [21] (deposition of Co nanocrystals).

balt nanocrystals. The field strengths used to produce the mesostructures of these nanocrystals range between 0.3 and 0.8 T (marked by an arrow). At these field strengths, the relationship between M and H is completely nonlinear. The aim of this paper is to develop a theory that takes the nonlinear behavior of $M(H)$ into account. Such a theory is of more general interest. Thus, the good agreement between theory and experiment observed in our recent paper [18] leads to the question: Why does a *linear* approach give reliable predictions, even at a high field, for the experiments carried out by Rosensweig *et al.*? Indeed, the magnetization curve of a typical ferrofluid shown in Fig. 1 indicates that some of those experiments in Hele-Shaw cells are carried out under nonlinear conditions.

How must the linear approach described in Ref. [18] be modified to take the nonlinear behavior of $M(H)$ into account? The morphology and size of the patterns are usually calculated by a minimization of the free energy. For a given structure (described in Sec. II A) the total energy is obtained by the following procedure in the linear case.

(1) From a given magnetization, the demagnetization field in the pattern is computed (see Sec. II C).

(2) The magnetization is calculated self-consistently from the demagnetization field using a linear relationship.

(3) The magnetization is used to evaluate the magnetic energy. Here, an equation is used, which is only valid in the linear case.

(4) The total free energy is calculated from the magnetic, surface and entropic terms.

In the nonlinear case, the nonlinear relationships have to be used in steps (2) and (3) as explained in Secs. II D and II E, respectively. This leads to some difficulties in step (3) (computation of the magnetic energy). In Sec. II E, we show how these problems can be solved. In Sec. III, the nonlinear theory is applied to calculate pattern size as a function of the field strengths. The nonlinear results are compared with the linear values and experimental data. Then, the theoretical results obtained by the nonlinear approach are discussed with respect to two limits. First, at low field strengths, the differences between the linear and nonlinear curves can be described by truncated expansions. Second, we can derive simplifying relationships at high field strengths, where the magnetization reaches a constant value. Finally, the transition between hexagonal and striped patterns is investigated. In particular, we are interested in the question, whether the nonlinear theory leads to new transitions with respect to the linear theory. All calculations were carried out using the homemade FORTRAN package $\mathcal{HEXALAB}$ [22].

II. THEORY

A. Description of the magnetic patterns

Following previous studies [3,10,18,19], the labyrinth is described as a repeating pattern of infinitely long parallel stripes, while the hexagonal structure is idealized as a hexagonal array of cylinders. The symmetries of these structures allow a marked reduction of the computing time. Therefore, very accurate estimates of the free energy can be calculated. Theoretical studies of realistic labyrinthine patterns have shown that the idealized description of the structures used here can give reasonable estimates of the pattern size [16].

The ratio of the ferrofluid to the total volume is denoted by ϕ. For a given ϕ, the geometry of the striped patterns is defined by the cell height L and by the stripe width w_f. The hexagonal structure is described by ϕ, L and r_0, which is the radius of the cylinders. The global frame is chosen in such a way that its x axis is along the direction of the applied field.

B. Free energy of ferrofluid patterns

In accordance with Refs. [3,10,18,19], values of r_0 or w_f are obtained by a minimization of the free energy per surface area $f=F/s$. The free energy consists of a surface and a magnetic term:

$$F=F_s+F_m. \tag{1}$$

Since we limit our study to pattern heights greater than 2 μm, the entropy is neglected [18]. The surface energy is characterized by the interfacial tension σ between the two immiscible liquids. In agreement with experimental studies [23], we assume that σ does not depend on the field strength. The surface energies per surface area for the hexagonal and striped patterns were derived elsewhere [see Eqs. (15) and (16) in Ref. [18]].

The general equation for the magnetic energy is given by

$$F_m=\int_V\int_0^B \mathbf{H}'(\mathbf{r})\cdot d\mathbf{B}'(\mathbf{r})d\mathbf{r}-\frac{\mu_0}{2}\int_V \mathbf{H}_0^2 d\mathbf{r}. \tag{2}$$

The magnetic induction is calculated from

$$\mathbf{B}(\mathbf{r})=\mu_0(\mathbf{H}(\mathbf{r})+\mathbf{M}(\mathbf{r})), \tag{3}$$

where $\mathbf{M}(\mathbf{r})$ is the magnetization in the cylinders or stripes.

The magnetization in the pattern is a function of the magnetic field

$$\mathbf{M}(\mathbf{r}) = f(\mathbf{H}(\mathbf{r})). \tag{4}$$

$\mathbf{H}(\mathbf{r})$ is the total field which is the sum of the strength of the applied field $\mathbf{H}_0$ and of the negative demagnetization field $\mathbf{H}_d(\mathbf{r})$:

$$\mathbf{H}(\mathbf{r}) = \mathbf{H}_0 + \mathbf{H}_d(\mathbf{r}). \tag{5}$$

C. Calculation of the demagnetization field

The demagnetization field is caused by the magnetization within the ferrofluid, which is calculated here from a nonlinear relation. The calculation of $\mathbf{H}_d$ from a given magnetization does not change in comparison with the linear case. It is explained elsewhere [18,19]. In particular, the correct treatment of the long-range dipolar interaction is derived in Ref. [18]. The volume-averaged magnetization is used during the evaluation of $\mathbf{H}_d$. This allows us to simplify the numerical calculations and, thus, to largely reduce the computing time [19]. We have recently shown that in the linear case this approximation does not significantly change the calculated pattern sizes and energies [19]. We also verified that in the nonlinear case the use of an averaged magnetization does not affect the theoretical results.

D. Nonlinear magnetization curves

In contrast to previous approaches, we do not restrict ourselves to a linear relationship between $\mathbf{M}$ and $\mathbf{H}$.

The magnetization curve $f(H)$ can be measured by experiments, such as those using the superconducting quantum interference device (SQUID). In this paper, it is approximated by a Langevin function, which is introduced in the following.

For ferrofluids with weak dipolar coupling, the magnetic interactions between the nanoparticles can be neglected. In this case, the Langevin theory gives reasonable estimates of the magnetization as a nonlinear function of the total magnetic field:

$$\frac{M_L(H)}{\varphi M_d} = L(\alpha) = \coth\alpha - \frac{1}{\alpha}, \tag{6}$$

$$\alpha = \frac{\pi}{6}\frac{\mu_0 M_d d^3}{k_B T} H. \tag{7}$$

We assume a monodisperse suspension of nanoparticles with a magnetic diameter d. M_d is the saturation moment of the bulk. φ is the volume fraction of the magnetic particles. Note the difference between φ and the ratio of the ferrofluid to the total volume in the pattern denoted by ϕ. φ can be calculated from the saturation moment of the ferrofluid M_s using $\varphi = M_s/M_d$. The temperature T is fixed at 300 K in the following.

We will use the Langevin model to study the influence of a nonlinear magnetization on the ferrofluid patterns. Therefore, we are now demonstrating that the use of a Langevin function is justified for the systems studied in the paper. To evaluate the effect of the approximations made in this model, we compare the magnetization curves of the Langevin and more accurate approaches. Several models have been derived to take the magnetic interparticular interactions into account [24–26]. For example, in the higher-order, modified, mean-field model [26], the field H in Eq. (7) is replaced by an effective field given by

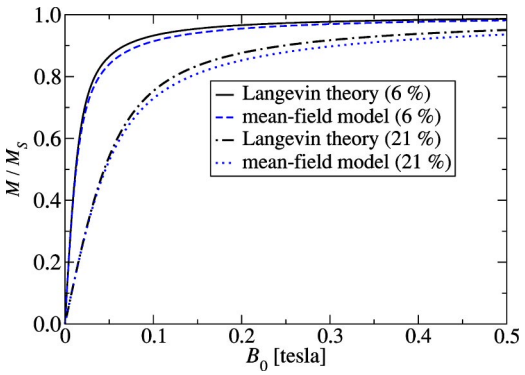

FIG. 2. Magnetization curves of a ferrofluid (magnetite particles with volume fractions of 6% and 21%, initial magnetic susceptibility of 1.6). Solid and dashed-dotted lines: Langevin function; dashed and dotted lines: modified mean-field model.

$$H_e = H + \frac{M_L(H)}{3} + \frac{1}{144} M_L(H) \frac{dM_L(H)}{dH}. \tag{8}$$

The range of validity of this theory is determined by the dipolar coupling parameter:

$$\lambda = \frac{m^2}{4\pi\mu_0 k_B T d^3}, \tag{9}$$

where the dipole moment of the magnetic particles is calculated from $m = \mu_0 M_d d^3 \pi/6$. A very recent simulation study has shown that the modified mean-field model gives reliable predictions for the dipolar coupling parameter $\lambda < 3$ [27]. Here, we restrict our study to values of λ smaller than 2.5 which corresponds to a particle size of about 12 nm. Figure 2 compares the magnetization curves obtained by the Langevin theory and the more accurate mean-field model. The initial susceptibility χ defined by the relationship $M = \chi H$ is fixed at 1.6. Two values of the volume fraction φ are used (6% and 21%) [27]. This covers the typical concentration range which is obtainable in real ferrofluids. The deviations between the two theories are less than 3%. This precision is sufficient for this study. Moreover, the Langevin function allows the use of analytical expressions to describe the evolution of the magnetization at intermediate field strength. This is used in Sec. III C.

For small field strengths ($\alpha \ll 1$), we reach a linear relationship between M and H characterized by the magnetic susceptibility. In the case of the Langevin theory the susceptibility is given by

$$\chi_L = \frac{\pi}{18}\varphi\frac{\mu_0 M_d^2 d^3}{k_B T}. \tag{10}$$

More accurate expressions were derived using the mean-spherical approximation (MSA) [28], the Born-Mayer expansion method [29], and the statistical model based on the pair correlation function [30]. Taking χ_L as a parameter, all the above approaches lead to the same higher-order expression for the initial susceptibility [30]:

$$\chi = \chi_L(1+\chi_L/3+\chi_L^2/144). \tag{11}$$

This equation corresponds to the weak field limit of the mean-field model [Eq. (8)]. Experimental measurements [30] and simulation studies [27] have shown that this equation gives reliable results for $\lambda<3$. In Sec. III A, Eqs. (10) and (11) will be employed to calculate the variation of the volume fraction φ of the magnetic fluid as a function of the particle size for given χ and M_d.

E. Calculation of the magnetic energy in the nonlinear case

In the case of a linear relationship between **M** and **H** Eq. (2) simplifies to give

$$F_m = -\frac{\mu_0}{2}\int_{V_m}\mathbf{M}(\mathbf{r})\cdot\mathbf{H}_0 d\mathbf{r}, \tag{12}$$

where V_m is the volume occupied by the magnetic liquid. There are two major differences between the general Eq. (2) for F_m and its linear counterpart.

(i) Equation (2) implies an additional integration over **B**.

(ii) The integrals of the general expression are over the total volume V, while in the linear equation they are only over the volume V_m of the magnetic matter.

These two differences markedly complicate the calculation in the nonlinear case. In the following section, we will show how they can be overcome.

For a nonlinear relationship $M=f(H)$, Eq. (2) cannot be simplified as in the linear case. In particular, the integration over **B** cannot be avoided. Thus, to obtain the magnetic energy for a given applied field H_0, the magnetization and the demagnetization field at all intermediate field strengths between 0 T and H_0 must be computed. In contrast in the linear case, the magnetization needs only to be evaluated at the field H_0. Tests have shown that we can use quite a large integration step $\Delta B<0.005$ T, without affecting the numerical precision of the results. In addition, the evolution of patterns is usually studied over a complete range of field strengths starting from 0 T. Therefore, the integration over **B** does not markedly reduce the efficiency of our approach.

The second difficulty arising from the use of Eq. (2) is due to the integration over the total volume. In the following, we will show that Eq. (2) can be rewritten in a form that contains only integrals over the magnetic volume as in the linear case. The first integral in Eq. (2) can be divided into two integrals, that over the volume of the magnetic fluid V_m and that of the nonmagnetic liquid V_{nm}:

$$F_m = \underbrace{\int_{V_m}\int_0^B \mathbf{H}'\cdot d\mathbf{B}'\,d\mathbf{r}}_{E_1} + \underbrace{\mu_0\int_{V_{nm}}\int_0^H \mathbf{H}'\cdot d\mathbf{H}'\,d\mathbf{r}}_{E_2} - \frac{\mu_0}{2}\int_V \mathbf{H}_0^2 d\mathbf{r}, \tag{13}$$

where we use that $\mathbf{B}=\mu_0\mathbf{H}$ in V_{nm}. After carrying through the integration over **H**, we can rewrite E_2 as

$$E_2 = \frac{\mu_0}{2}\int_V H^2 d\mathbf{r} - \frac{\mu_0}{2}\int_{V_m} H^2 d\mathbf{r}. \tag{14}$$

The integral over V_{nm} in Eq. (13) is replaced by the difference of those over the total volume V and V_m. In order to further simplify E_2, we use a relationship derived in Rosensweig's textbook ([1], pp. 96–98):

$$\int_V \frac{1}{2}(\mathbf{B}\cdot\mathbf{H}-\mu_0\mathbf{H}_0^2)d\mathbf{r} = -\frac{\mu_0}{2}\int_{V_m}\mathbf{M}\cdot\mathbf{H}_0 d\mathbf{r}. \tag{15}$$

This relationship also holds in the nonlinear case, because for its derivation the assumption of a linear relationship between **M** and **H** is not used. Employing $\mathbf{B}=\mu_0(\mathbf{H}+\mathbf{M})$, Eq. (15) can be rearranged to give

$$\frac{\mu_0}{2}\int_V H^2 d\mathbf{r} = -\frac{\mu_0}{2}\int_V \mathbf{M}\cdot\mathbf{H} d\mathbf{r} + \frac{\mu_0}{2}\int_V \mathbf{H}_0^2 d\mathbf{r} - \frac{\mu_0}{2}\int_{V_m}\mathbf{M}\cdot\mathbf{H}_0 d\mathbf{r}. \tag{16}$$

The first integral on the right side can be restricted to V_m, since $\mathbf{M}=0$ outside the magnetic liquid. Combining Eqs. (13), (14) and (16), we finally arrive at

$$F_m = \int_{V_m}\int_0^B \mathbf{H}'\cdot d\mathbf{B}'\,d\mathbf{r} - \frac{\mu_0}{2}\int_{V_m}\mathbf{M}\cdot\mathbf{H} d\mathbf{r} - \frac{\mu_0}{2}\int_{V_m}\mathbf{M}\cdot\mathbf{H}_0 d\mathbf{r} - \frac{\mu_0}{2}\int_{V_m} H^2 d\mathbf{r}. \tag{17}$$

The new form of F_m is very useful in computation since it contains only integrals over V_m. This largely reduces the size of the spatial grid used for the numerical integration. In the case of the hexagonal pattern, another fact makes Eq. (17) very useful for the numerical calculations which is explained as follows. Let us study the evolution of the demagnetization field in the hexagonal pattern. The demagnetization field is used to calculate the total field, which appears in the equation of the magnetic energy. The demagnetization field is self-consistently computed by an integration over the magnetization as discussed in Sec. II C. The magnetization is calculated from a Langevin function introduced in Sec. II D. We use the same parameters for the Langevin function as in the whole paper. The demagnetization field is plotted as a

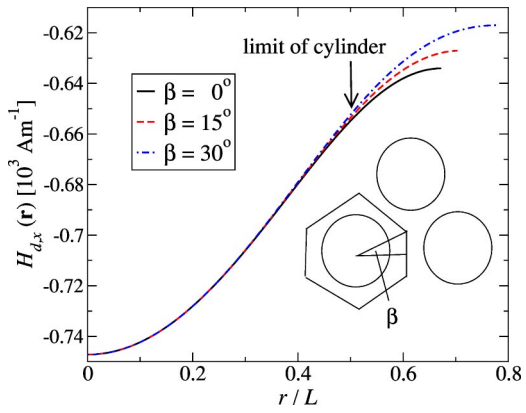

FIG. 3. Demagnetization field as a function of the distance from the cylinder center for three values of β. Parameters: $B_0=0.002$ T, $\chi=1.6$, $\phi=0.5$, $r_0=0.5$ mm, $L=1$ mm, and $x=0$. The sketch presents a cylinder and two of its neighbors. The hexagon indicates the average space around the central cylinder used to carry out the integration.

function of the distance from the center of a cylinder in Fig. 3. The sketch in the same figure shows the tops of three cylinders of the hexagonal pattern. Due to the translational symmetry of the idealized structure, the integrals over the total volume in Eq. (2) can be restricted to the hexagon around one cylinder. In Fig. 3, we plot only the evolution of the demagnetization field within the hexagon. β denotes the radial angle of the cylindrical frame with its origin at the center of a cylinder. Due to the rotational symmetry of the hexagonal pattern, the calculations can be restricted to the interval of 30° presented by the two lines within the hexagon of Fig. 3. $\beta=0°$ denotes the direction of the smallest separation from the next cylinder, while $\beta=30°$ corresponds to the midway between two neighboring dots. The number of angles β necessary for an accurate computation of the integrals in Eqs. (2) and (17) depends on the variation of $\mathbf{H}_d$ with β. Figure 3 shows that outside the cylinder the demagnetization fields for the different values of β deviate. Therefore, in the case of Eq. (2) where we integrate over the total volume many angles β have to be used. In contrast, the variation of $\mathbf{H}_d$ with β is small within the limits of the cylinder. For Eq. (17), where the integration is restricted to the inside of the cylinder, we can therefore reduce the number of angles β. We want to emphasize that the use of Eq. (17) instead of the general expression does not only lead to an enormous gain in computing time. In addition, only the reformulated equation allowed an accurate computation of the magnetic energies. Indeed, we never did succeed in the calculation of numerically stable values of F_m from Eq. (2) for hexagonal patterns even when very large numbers of β values were used. Hence, the use of Eq. (17) instead of the original expression makes possible an accurate and efficient calculation of the magnetic term.

There are several other approximation schemes proposed in the literature to calculate the magnetic energy in the linear case. We have recently shown that the approximation of an average magnetization for the demagnetization field used here gives the best results in comparison with accurate values [18]. Therefore, we will restrict our study to this approximation. It is nevertheless interesting to note that an alternative approach introduced by Cebers and recently used in Ref. [31] can be easily extended to the nonlinear case. This approach assumes a constant magnetization during the pattern formation. It has been demonstrated that this approach can be derived as an approximation of the method using an average magnetization. Nevertheless, the pattern size obtained by the constant approach is in good agreement with accurate results in the linear case. The constant magnetization could be calculated from a nonlinear magnetization curve, such as in Eq. (6), and, thus, this approach could be also applied in the nonlinear case. We expect that this method gives pattern size in good agreement with the approach used here, since it can be shown that the results are close at low and high field. Actually, at low field, we will find the good agreement for the linear case discussed above. At high field saturation, we will show in Sec. III C that the equations of magnetic energy for both approaches become the same.

TABLE I. Values of the volume fraction of magnetic particles φ in the ferrofluid calculated from Eqs. (10) and (11) for different particle sizes. $\chi=1.6$; $M_d=4.46\times10^5$ A m^{-1}.

d (nm)	φ, Langevin	φ, mean-field
6	69.0%	50.5%
8	29.5%	21.2%
10	15.1%	10.8%
12	8.7%	6.2%

III. RESULTS

A. The influence of the nonlinear magnetization curve on the pattern size

To compare the pattern sizes predicted by a linear and a nonlinear approach, the magnetization curve is represented by the Langevin function in Eq. (6). The comparison in Fig. 2 has shown that the Langevin theory gives reliable predictions under the conditions studied here. Since the magnetic particles in many ferrofluids consist of magnetite, the domain magnetization of this material is used in the following ($M_d=4.46\times10^5$ A m^{-1}). The initial magnetic susceptibility, measured by Rosensweig *et al.* [3] for the ferrofluid employed in their experiment, is 1.6. The interfacial tension, the volume fraction, and the cell height correspond to the experimental conditions published in the same Ref. [3] ($\sigma=0.0043$ N m^{-1}, $\phi=0.5$, $L=0.9$ mm). The particle diameter d in normal ferrofluids is about 10 nm [32]. The magnetization curve calculated from the Langevin function for this particle diameter is shown in Fig. 1. To study the influence of the particle size, four different diameters d ranging from 6 nm to 12 nm are used. From M_d, χ and d, the magnetic volume fraction φ within the ferrofluid can be calculated either by Eq. (10) or by the more accurate mean-field equation (11). The results of φ for the four particle sizes studied here are shown in Table I. While particle sizes around 10 nm yield reasonable values of φ, the volume fraction of 50.5% obtained for $d=6$ nm is unrealistically large.

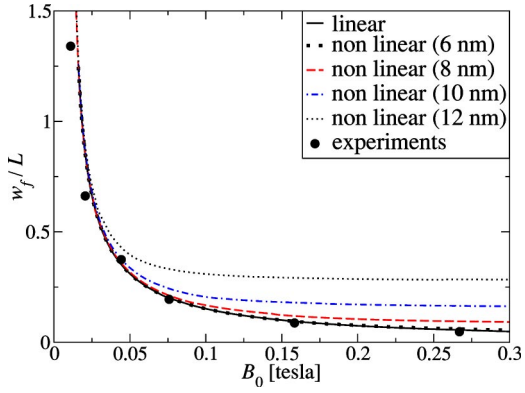

FIG. 4. Dependence of the normalized stripe width w_f/L in striped structures on the external field H_0. The theoretical results of the linear and the nonlinear methods are compared to experimental data. The nonlinear curves are shown for four different particle sizes. Parameters: $\chi=1.6$, $M_d=4.46\times10^5$ A m^{-1}, $L=0.9$ mm, $\phi=0.5$, and $\sigma=0.0043$ N m^{-1}. The experimental points were obtained from Ref. [3]. The curve for $d=6$ nm deviates only at a high field from the linear one.

We will come back to this point, when we compare the nonlinear results with the experimental data.

Figure 4 shows the energetically favorable stripe width as a function of the applied field H_0. The dots in this figure correspond to the experimental data taken from Ref. [3]. The comparison between the linear and the nonlinear curves leads to the following conclusions. First, the effect of the nonlinearity of $M(H)$ markedly depends on the particle size. Thus, for $d=6$ nm we observe only small differences between the linear and the nonlinear curve for the studied fields. With increasing particle size the deviation from the linear behavior increases. Second, the nonlinear curves saturate at high field, which can be observed in Fig. 4 for $d=10$ nm and 12 nm. This behavior is in contrast with the linear case where saturation is not expected for the following reason. It has been shown elsewhere that a diminution of the pattern size always leads to a decrease of the demagnetization field [4]. This change in the demagnetization field causes a larger magnetization and a more negative energy according to Eq. (12), which explains the pattern formation. This works even at high field in the linear case. For the same reasons, a saturation is expected for a nonlinear relation, since M cannot be changed by a variation of the demagnetization field at high field. Therefore, a further reduction of the pattern size does not lead to a more negative energy and the nonlinear curves saturate. For smaller particle diameters, the saturation limit is reached at higher field strengths and cannot therefore be observed in Fig. 4.

The two conclusions drawn from Fig. 4 are also valid for the magnetization curves calculated from the Langevin function (see Figs. 1 and 2). Obviously, the pattern sizes are markedly determined by the form of $M(H)$. In contrast, the magnetization curves of the Langevin equation cannot directly be used to predict the onset of the nonlinear behavior. Thus, for $d=10$ nm the nonlinear curve in Fig. 4 deviates from the linear one at $H_0=0.03$ T. In Fig. 1, we observe the transition to a nonlinear behavior at lower field strengths of about 0.015 T. This can be explained as follows. The ferrofluid forming the pattern is subjected to a field which is reduced from the applied field strength due to the demagnetization field. Since the magnetization in the pattern depends on the total field, the applied field in Fig. 4 must be higher than that in Fig. 1 to compensate the demagnetization field and to induce a nonlinear behavior. Due to this demagnetization effect, the linear theory for the field-induced patterns is expected to give reasonable results over a larger range than the linear approximation of the Langevin function.

B. Comparison with experimental data

We have recently shown that a linear approach, which takes the nonuniformity of the magnetization in the patterns into account, correctly describes the decrease in the pattern size at a high field. For the comparison between the nonlinear results and the experimental data, we face a serious problem. Rosensweig *et al.* [3] do not give enough information to completely define the magnetization curve. They only mention the initial susceptibility of 1.6 and the saturation magnetization of 25860 A m^{-1}. Assuming the material of the particles is magnetite, a volume fraction can be computed from equation $\varphi=M_s/M_d=5.8\%$. Using the mean-field equation (11) with the given value of χ gives a particle diameter of 12.3 nm. [The Langevin expression (10) yields a larger value of $d=13.8$ nm.] Figure 4 shows that the results obtained for $d=12$ nm markedly deviate from the experimental data points. We have investigated several reasons to explain this disagreement.

First, a particle size of 12 nm seems to be quite large in comparison with diameters typically published in the literature, which vary between 6 and 10 nm [32]. The choice of a smaller particle diameter of about 6 nm markedly improves the agreement with the experimental data. However, a diameter of the order of 6 nm implies unreasonably large volume fractions of 50%. Another reason for the disagreement between the experiment and the nonlinear approach might be the use of the Langevin theory. However, we found that the magnetization curve obtained from the mean-field expression is very close to the Langevin function (see Fig. 2). Thus the use of the Langevin function cannot explain the deviations from the experiment. We have also examined the idea that the particles are not made of magnetite. A thorough study of Eqs. (6), (7), and (11) shows that α is completely defined by the values of M_s and χ. This means that we can use any value of M_d without changing the magnetization curve calculated from the Langevin equation. However, the dipolar coupling parameter increases with M_d and the Langevin theory might not give reliable predictions for the magnetization in this case. Without further information on the magnetization curve of the ferrofluid we cannot reach a conclusion as to the quality of the nonlinear approach. Nevertheless, experimental studies, which were recently carried out at our laboratory [21], indicate that the nonlinear approach is able to correctly predict pattern sizes at a high field. In particular, the existence of a high-field saturation is shown by these experiments.

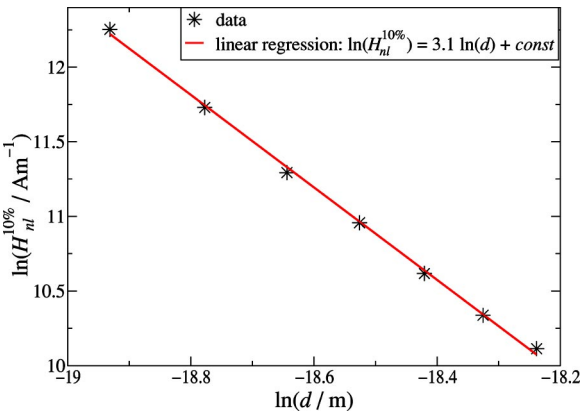

FIG. 5. Logarithms of the magnetic field where the linear and nonlinear curves deviate more than 10% as a function of the logarithm of the particle diameter. The diameter varies between 6 and 12 nm. The solid line shows a linear fit of the calculated points. Parameters: see Fig. 4.

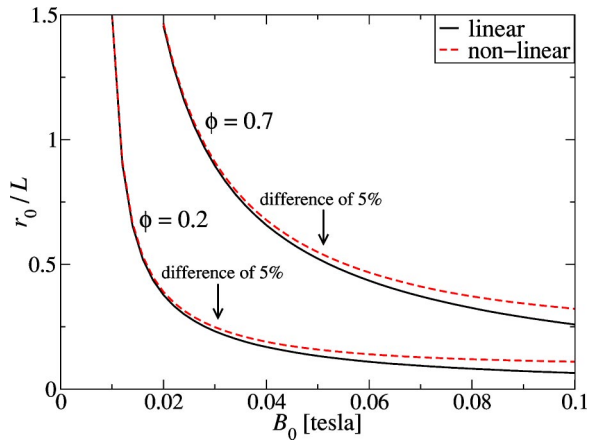

FIG. 6. Dependence of the normalized cylinder radius r_0/L for hexagonal structures on the external field H_0. The theoretical results of the linear and the nonlinear methods are compared. The particle diameter is $d=10$ nm. Parameters: $\chi=1.6$, $M_d=4.46\times10^5$ A m^{-1}, $L=1$ mm, $\phi=0.5$, and $\sigma=0.0043$ N m^{-1}.

C. Limiting cases of the nonlinear theory

It is of interest to examine the asymptotic behavior of the nonlinear approach at low and high field. For low field strength, the results are those of the linear theory. Figure 4 shows that the field, at which nonlinear and linear results begin to deviate, strongly depends on the particle size. In order to study this dependence, we have defined $H_{nl}^{10\%}$ as the field, at which the difference between the nonlinear and linear values of w_f is 10%. Figure 5 is a ln-ln plot of $H_{nl}^{10\%}$ as a function of the particle size d. The parameters are the same as in Fig. 4. The solid line represents a linear fit of the data. Obviously, $H_{nl}^{10\%}$ decreases roughly as the inverse of the third power of d: $H_{nl}^{10\%}\propto d^{-3}$. This is explained by a development of the Langevin function up to the second term

$$L(\alpha)=\frac{\alpha}{3}-\frac{\alpha^3}{45}+O(\alpha^5). \tag{18}$$

Using Eq. (7) for α, we find for a deviation of x% from linearity for the Langevin function:

$$x\%\approx-\frac{\alpha^3}{45}\propto d^6(H_{nl}^{x\%})^2. \tag{19}$$

Rearranging the terms we arrive at

$$\ln x\%\propto 2\ln d^3+2\ln(H_{nl}^{x\%})\rightarrow H_{nl}^{x\%}\propto d^{-3}. \tag{20}$$

Obviously, the beginning of nonlinear effects is determined by the form of the magnetization curve. In the previous section, however, we have observed that the demagnetization field modifies the onset of the nonlinear behavior. This is evident, when the pattern size is studied at various volume fractions. Figure 6 is the plot of the cylinder radius for hexagonal patterns at $\phi=0.2$ and $\phi=0.7$. For the larger volume fraction, the nonlinear curve starts to deviate from the linear one at much higher field strengths (see arrows in Fig. 6). This can be explained by the demagnetization effect. For larger ϕ, the cylinders are closer and the demagnetization field is higher than for small ϕ. Therefore, the applied field must be larger to compensate the demagnetization effect and to give a nonlinear behavior.

At a high field, the magnetization of the ferrofluid reaches its saturation value M_s. Then, the magnetization is constant during the pattern formation. In this case, it has been shown that the calculation of the magnetic energy can be greatly simplified [14,18].

$$F_m=\sum_{i=1}^{N_0}\frac{M_s^2\mu_0}{4\pi}\int dy_1dz_1\int dy_idz_i \times\left\{\frac{1}{\sqrt{(\mathbf{s}_1-\mathbf{s}_i)^2}}-\frac{1}{\sqrt{(\mathbf{s}_1-\mathbf{s}_i)^2+L^2}}\right\}. \tag{21}$$

The sum is over all cylinders or stripes in the pattern. $\mathbf{s}_i=(y_i,z_i)$ denotes points at the top of the cylinder or stripe i.

The new expression is derived from the interpretation of the magnetic potential as that arising from constant magnetic charges along the top and the bottom surfaces of the magnetic domains (see the discussion of method C in Ref. [18]). We have verified that the stripe widths obtained by the nonlinear approach actually tend to the results calculated from expression (21) at a high field.

D. Transition between hexagonal and labyrinthine patterns

The transition between hexagonal and labyrinthine patterns was observed in several experiments [5–7]. These indicate that hexagonal structures predominate at small ϕ. This has been explained by theoretical studies [11,18,33]. In contrast, our linear theory does not account for the transition between both structures experimentally observed by a variation of the external field. Two different explanations for these field-induced transitions have been proposed in the literature. Hong *et al.* [34] gave experimental evidence that the transition between hexagonal and labyrinthine patterns observed at small ϕ is due to metastable structures. In contrast, Lacoste

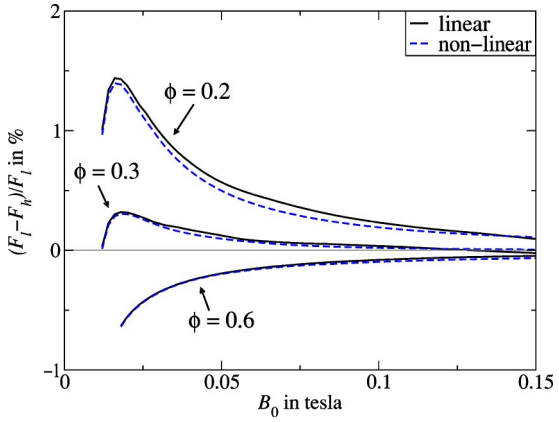

FIG. 7. Normalized free energy differences $(F_l-F_h)/F_l$ as a function of the field for three representative ratios ϕ of the magnetic to the total volume. The results for the nonlinear and the linear approach are given. Parameters: $\chi=1.6$, $M_d=4.46\times10^5$ A m^{-1}, $d=10$ nm, $L=1$ mm, and $\sigma=0.0043$ N m^{-1}.

and Lubensky [11] explain the field-induced transitions using a model with a varying density of magnetic nanoparticles within the ferrofluid. With respect to this discussion, it is of some interest whether the nonlinearity of the magnetization curve can lead to new transitions between hexagonal and labyrinthine patterns. In Fig. 7 the normalized energy difference $(F_l-F_h)/F_l$ in % between the labyrinthine and hexagonal patterns is plotted. The positive values of $(F_l-F_h)/F_l$ for $\phi<0.3$ indicates the predominance of hexagonal patterns at small volume fraction. For the particle diameter of 10 nm used here, Fig. 1 shows that differences between the nonlinear and linear results can be expected at fields larger than 0.05 T. The observed differences are small. In particular, no transition is observed by a variation of the field using both approaches. At a high field, the nonlinear theory reaches a constant difference $(F_l-F_h)/F_l$ due to the saturation limit.

IV. CONCLUSIONS

We have developed a theory for the prediction of patterns in ferrofluid films using nonlinear magnetization curves. A reformulation of the magnetic energy term provides accurate and efficient calculations of the free energy. This enables the study of ferrofluid patterns even at a high field.

The theoretical results are strongly determined by the form of the magnetization curve. Thus, the field, at which a nonlinear behavior begins, increases with $1/d^3$ as the Langevin function. Moreover, a saturation is observed at a high field which is typical for a nonlinear behavior. The theoretically predicted saturation regime has been confirmed by recent experiments [21]. We have shown here that at saturation a simplified formula of the magnetic energy can be used.

In spite of the predictive value of the magnetization curve, it cannot be used to estimate the field where the nonlinear curve separates from the linear one. This is due to the demagnetization field, which shifts the beginning of nonlinearity to higher fields. Therefore, the linear theory of pattern formation should be reliable over a larger field range than in the case of the magnetization curve. For the transition between hexagonal and labyrinthine patterns, only small differences have been observed between the linear and nonlinear approaches.

The comparison with experiments suffers from the lack of reliable data on the magnetization curve of the experimentally used ferrofluid. Our approach predicts an agreement between the nonlinear and linear theory only at unrealistically small particle diameters. Therefore, we do not understand the success of the linear theory in reproducing the experimental data for the time being. More experimental data on ferrofluid patterns, in particular at high field strength, would be of great value.

ACKNOWLEDGMENTS

The authors thank Adrien Fuchs for his important contributions to this work. The authors also gratefully acknowledge the fruitful discussions with Dr. D. Ingert and V. Germain. They wish to thank V. Germain and Dr. C. Petit who measured the magnetization curve of the cobalt nanoparticle deposition published here.

[1] R.E. Rosensweig, *Ferrohydrodynamics* (Dover, Mineola, NY, 1997).
[2] A. Cebers and M.M. Maiorov, Magnetohydrodynamics (N.Y.) **16**, 21 (1980).
[3] R.E. Rosensweig, M. Zahn, and R. Shumovich, J. Magn. Magn. Mater. **39**, 127 (1983).
[4] J. Richardi, D. Ingert, and M.P. Pileni, J. Phys. Chem. B **106**, 1521 (2002).
[5] J.-C. Bacri, R. Perzynski, and D. Salin, Endeavour **12**, 76 (1988).
[6] F. Elias, C. Flament, J.-C. Bacri, and S. Neveu, J. Phys. I **7**, 711 (1997).
[7] C.-Y. Hong, I.J. Jang, H.E. Horng, C.J. Hsu, Y.D. Yao, and H.C. Yang, J. Appl. Phys. **81**, 4275 (1997).
[8] Y. Grasselli, G. Bossis, and E. Lemaire, J. Phys. II **4**, 253 (1994).
[9] J. Liu, E.M. Lawrence, A. Wu, M.L. Ivey, G.A. Flores, K. Javier, J. Bibette, and J. Richard, Phys. Rev. Lett. **74**, 2828 (1995).
[10] F.M. Ytreberg and S.R. McKay, Phys. Rev. E **61**, 4107 (2000).
[11] D. Lacoste and T.C. Lubensky, Phys. Rev. E **64**, 041506 (2001).
[12] S.A. Langer, R.E. Goldstein, and D.P. Jackson, Phys. Rev. A **46**, 4894 (1992).
[13] A.J. Dickstein, S. Erramilli, R.E. Goldstein, D.P. Jackson, and S.A. Langer, Science **261**, 1012 (1993).
[14] D.P. Jackson, R.E. Goldstein, and A.O. Cebers, Phys. Rev. E **50**, 298 (1994).

[15] A. Cebers and I. Drikis, Magnetohydrodynamics (N.Y.) **32**, 11 (1996).
[16] I. Drikis, J.-C. Bacri, and A. Cebers, Magnetohydrodynamics (N.Y.) **35**, 203 (1999).
[17] M. Seul and D. Andelman, Science **267**, 476 (1995).
[18] J. Richardi, D. Ingert, and M.P. Pileni, Phys. Rev. E **66**, 046306 (2002).
[19] J. Richardi and M.P. Pileni (unpublished).
[20] J. Legrand, A.T. N'Go, C. Petit, and M.P. Pileni, Adv. Mater. **18**, 53 (2001).
[21] V. Germain, J. Richardi, D. Ingert, and M.P. Pileni (unpublished).
[22] The Fortran package $\mathcal{HEXALAB}$ is a highly optimized code of about ten thousands statements, which calculate the geometry and energy of magnetic fluid patterns. The kind of pattern is not restricted to hexagonal or labyrinthine ones. $\mathcal{HEXALAB}$ was developed by J. Richardi at the LM2N (direction: M.P. Pileni).
[23] C. Flament, S. Lacis, J.-C. Bacri, A. Cebers, S. Neveu, and R. Perzynski, Phys. Rev. E **53**, 4801 (1996).
[24] J.-C. Bacri, A. Cebers, A. Bourdon, G. Demouchy, B.M. Heegaard, and R. Perzynski, Phys. Rev. Lett. **74**, 5032 (1995).
[25] J.-C. Bacri, A. Cebers, A. Bourdon, G. Demouchy, B.M. Heegaard, B. Kashevsky, and R. Perzynski, Phys. Rev. E **52**, 3936 (1995).
[26] A.F. Pshenichnikov, V.V. Mekhonoshin, and A.V. Lebedev, J. Magn. Magn. Mater. **161**, 94 (1996).
[27] Z. Wang, C. Holm, and H.W. Müller, Phys. Rev. E **66**, 021405 (2002).
[28] M.S. Wertheim, J. Chem. Phys. **55**, 4291 (1971).
[29] B. Huke and M. Lücke, Phys. Rev. E **62**, 6875 (2000).
[30] A.0. Ivanov and O.B. Kuznetsova, Phys. Rev. E **64**, 041405 (2001).
[31] A. Cebers, Phys. Rev. E **66**, 061402 (2002).
[32] B.M. Berkovsky, V.F. Medvedev, and M.S. Krakov, *Magnetic Fluids*, *Engineering Applications* (Oxford Science Publications, Oxford, 1993).
[33] A. Cebers, Magnetohydrodynamics (N.Y.) **31**, 61 (1995).
[34] C.-Y. Hong, C.-H. Lin, C.-H. Chen, Y.P. Chiu, S.Y. Yang, H.E. Horng, and H.C. Yang, J. Magn. Magn. Mater. **226**, 1881 (2001).